Tailoring the Selectivity of Ti-Based Photocatalysts (TiO2 and Microporous ETS-10 and ETS-4) by Playing with Surface Morphology and Electronic Structure

ARTICLE *in* CHEMISTRY OF MATERIALS · JUNE 2006

Impact Factor: 8.35 · DOI: 10.1021/cm052841g

8 AUTHORS, INCLUDING:

Paola Calza
Università degli Studi di Torino
85 PUBLICATIONS **1,661** CITATIONS
SEE PROFILE

Claudio Minero
Università degli Studi di Torino
329 PUBLICATIONS **8,126** CITATIONS
SEE PROFILE

Carlo Lamberti
Università degli Studi di Torino
382 PUBLICATIONS **13,135** CITATIONS
SEE PROFILE

A. Zecchina
Università degli Studi di Torino
560 PUBLICATIONS **20,089** CITATIONS
SEE PROFILE

Tailoring the Selectivity of Ti-Based Photocatalysts (TiO_2 and Microporous ETS-10 and ETS-4) by Playing with Surface Morphology and Electronic Structure

Sandro Usseglio,[†,‡] Paola Calza,[‡,§] Alessandro Damin,[†,‡] Claudio Minero,[‡,§] Silvia Bordiga,[†,‡] Carlo Lamberti,[†,‡] Ezio Pelizzetti,*[,‡,§] and Adriano Zecchina*[,‡]

Dipartimento di Chimica IFM, Università di Torino, Via P. Giuria 7, I-10125 Turin, Italy, INSTM Unità di Torino Università, Turin, Italy, Dipartimento di Chimica Analitica, Università di Torino, Via P. Giuria 5, I-10125 Turin, Italy, and NIS Centre of Excellence, Università di Torino, Torino, Italy

Received December 23, 2005. Revised Manuscript Received May 2, 2006

In the first part of this work we report an exhaustive characterization of the bulk and surface properties of ETS-4 and ETS-10 microporous titanosilicates by means of combined N_2 volumetric measurements, SEM, IR, Raman, and UV−Vis techniques. The structure of the surface titanols, derived from literature XRD studies, is shown using a molecular graphic approach. UV−Vis titration experiments using H_2O_2, and catechol molecules, allowed us to directly measure the total number of available titanols (both in the channels and on the crystal external surface) and the surface titanols, respectively. In the second part of the paper, the ability of ETS-4 and ETS-10 (and of the standard P25) in the photodegradation of phenol (P), 4-chlorophenol (CP), 2,5-dichlorophenol (DCP), 2,4,5-trichlorophenol (TCP), 1,3,5-trihydroxybenzene (THB), and 2,3-dihydroxynaphthalene (DHN) is investigated, using both UV and visible lights, exciting above and below the materials energy gap, respectively. While microporous ETS-4 and ETS-10 exhibit a significant selectivity in the photodegradation of the above-mentioned molecules using both lights, P25 selectivity is observed with visible light only. This means that besides the inverse shape selectivity effect already observed for the microporous materials [Xamena et al. *J. Am. Chem. Soc.* **2003**, *125*, 2264], selectivity may be achieved also by selecting the excitation light in accordance with the electronic transition of the adsorbed molecule (determined by a previous systematic UV−Vis study). In such a case the photodegradation may occur if the conduction band of the Ti-based material is opportunely matched with the LUMO level of the adsorbed molecule so that it can receive the electron of the excited adsorbate. The concept of band alignment, well-established in the field of solid-state physics applied to semiconductor heterostructures [Margaritondo, G. *Rep. Prog. Phys.* **1999**, *62*, 765; Lamberti, C. *Surf. Sci. Rep.* **2004**, *53*, 1], is transferred to the field of photocatalysis for the first time.

1. Introduction

Photocatalysis has received enormous attention in recent years for its application in organic synthesis[1,2] or in the abatement of pollutants in water or in air.[3−6] TiO_2 is one of the most extensively studied photocatalysts for its application in several fields and in particular for its great performance in the oxidative photodegradation of different organic substrates.[7] The number of papers published has been strongly increasing through the years. From this point of view the topic can be considered as mature. However, it is a widespread opinion that an injection of nanoscience methods could give a new hint for innovation. One of the problems related to TiO_2 is the apparent absence of selectivity, which precludes the preferential degradation of only one given component from a mixture or its use as a selective photosynthetic catalyst.

Until now, only few papers[8−12] explicitly trying to overcome this problem have appeared. Following Inumaru's strategy,[8] selectivity is obtained by nanostructuring the TiO_2 surfaces by grafting *n*-octyltriethoxsylane groups. These groups act as hydrophobic centers, able to selectively adsorb molecules characterized by a specific mutual affinity. These molecules consequently are preferentially degraded in the

* Corresponding authors. A.Z.: tel., +39011-6707860; fax, +390116707855; e-mail, adriano.zecchina@unito.it. E.P.: tel., +3911-6707630; fax, +3911-6707615; e-mail, ezio.pelizzetti@unito.it.
† Dipartimento di Chimica IFM and INSTM.
‡ NIS Centre of Excellence.
§ Dipartimento di Chimica Analitica.

(1) Fox, M. A.; Chen, C. C.; Park, K.; Younathan, N. J. *ACS Symp. Ser* **1985**, *278*, 69−78.
(2) Fox, M. A. *Acc. Chem. Res.* **1983**, *16*, 314−321.
(3) Hoffman, M. R. *J. Phys. Chem.* **1987**, *91*, 3328−3333.
(4) Fox, M. A.; Dulay, M. T. *Chem. Rev.* **1993**.
(5) Pelizzetti, E.; Minero, C.; Pramauro, E. In *Chemical Reactor Technology for Environmentally Safe Reactors and Products*; de Losa, H. I., Ed.; Kluwer: Dortdrecht, 1993; p 577.
(6) Pelizzetti, E.; Minero, C. *Comments Inorg. Chem.* **1994**, *15*, 297−337.
(7) Carp, O.; Huisman, C. L.; Reller, A. *Prog. Solid State Chem.* **2004**, *32*, 33−177.
(8) Inumaru, K.; Murashima, M.; Kasahara, T.; Yamanaka, S. *Appl. Catal., B* **2004**, *52*, 275−280.
(9) Ghosh-Mukerji, S.; Haick, H.; Schvartzman, M.; Paz, Y. *J. Am. Chem. Soc.* **2001**, *123*, 10776−10777.
(10) Ghosh-Mukerji, S.; Haick, H.; Paz, Y. *J. Photochem. Photobiol., A* **2003**, *160*, 77−85.
(11) Calza, P.; Paze, C.; Pelizzetti, E.; Zecchina, A. *Chem. Commun.* **2001**, 2130−2131.
(12) Xamena, F.; Calza, P.; Lamberti, C.; Prestipino, C.; Damin, A.; Bordiga, S.; Pelizzetti, E.; Zecchina, A. *J. Am. Chem. Soc.* **2003**, *125*, 2264−2271.

10.1021/cm052841g CCC: $33.50
Published on Web 06/29/2006

TiO_2 patches located between the grafted organic groups. Following Ghosh's strategy,[9,10] selectivity is obtained via the formation of specific molecular sites for the recognition of the target molecule in the vicinity of titanium dioxide surface, from where they surface-diffuse to the photocatalytic TiO_2 domains. These sites are located on the surface of gold particles supported on TiO_2. The two strategies have significant similarities because both are obtained by modification at the nanolevel scale of the bare TiO_2 surface.

In previous works we have found that the selectivity can also be achieved using a Ti-based molecular sieve[11,12] (ETS-10) which is a nanostructured microporous material[13,14] characterized by the presence of one-dimensional linear chains of TiO_6 octahedra (−O−Ti−O−Ti−) behaving as semiconducting nanowires.[15−18] The combination of a wide band-gap semiconducting oxide with a three-dimensional 12-membered ring microporous framework offers many potential advantages in photocatalysis, such as excellent diffusion of reactant molecules, trapping, and in particular, shape selectivity. In the perfect structure these quantum wires are surrounded by an envelope of SiO_4 groups. These wires are characterized by full (O-based: 2p) valence and empty (Ti-based: $3d_{xy}$ and $3d_{z2}$) conduction bands,[17,18] separated by a band gap of about 4.03 eV, which is slightly higher than that of TiO_2 (3.2 eV) due to confinement effects. They can act as an antenna-like system able to collect the light and to form electron−hole pairs in the −O−Ti−O−Ti− chain. Like in TiO_2, these pairs can recombine or diffuse toward the wire to its end originating photocatalytic activity. In a perfect crystal, this happens where the wires emerge on the external surface, but in the real material this can happen also at internal defects (Ti vacancies). In the cited works[11,12] we have demonstrated three main features of the degradation process: (i) the photocatalytic active sites are titanols located on the external surfaces where the −O−Ti−O−Ti− chain emerges, exposing a surface Ti−OH titanol group; (ii) the fundamental role in determining the shape selectivity is played by the channels and channel mouth shape; (iii) both activity and selectivity can be improved by controlled defect production.[12] As a high selectivity toward the photodegradation of large aromatic molecules has been observed, it has been concluded that molecules entering the pore system were protected from photodegradation, which occurred on the external surface. The ETS-10 thus displays a peculiar inverse shape selectivity. The interpretation that the active photocatalytic centers are Ti−OH species at defective sites well agrees by the parallel studies by Howe's group,[19,20] which have shown how a highly defective proton-exchanged sample of ETS-10 was much more active for the gas-phase photooxidation of ethylene than a well-crystalline as-synthesized sample. The local structure of the actually involved Ti−OH sites and the photochemical mechanism are however still a matter of debate.

A substantial difference between ETS-10 and TiO_2 modified systems, previously mentioned,[8−10] lies in the fact that surface nanostructuring is in one case (ETS-10) a structural property, while in the other cases it is the result of an external intervention modifying the original properties. A second difference is represented by the band gap, definitely higher on ETS-10 with respect to TiO_2. This implies that the synthesis of solids containing quantum wire affords a method to tailor the band gap and to modulate the response to photons activations.[17]

All these strategies are exploiting the so-called "band-gap" (BG) mechanism and can be schematized as follows: the excitation is primarily created in the TiO_2 framework or in the −O−Ti−O−Ti− quantum wires by using photons with energy $h\nu \geq E_g$ (band gap) and photo selectivity is obtained: (i) by manipulating the structure of the surface sites where the electrons and the holes are transferred to the adsorbates[8−10] or (ii) by modifying the structure and the length of the embedded quantum wires.[11,12]

Selectivity may also be obtained following an alternative strategy based on the adsorbed molecular complex to solid "charge transfer" (CT) mechanism. Following this mechanism, the photons are absorbed not only by the solid itself but also by the isolated adsorbed complexes formed by interaction of the reactants with the surface. The photoactivation is then transferred from the excited surface complex to the conduction band of the solid, so initiating photoinduced transformations.[21,22] From this picture it can be inferred that adsorbates with appropriate charge transfer bands could be selectively degraded and transformed by choosing appropriate excitation frequencies. The two mechanisms are often simultaneously present and their relative contribution to the overall activity (and hence to selectivity) can be tailored by simultaneously operating on the structure of the adsorbing sites and on the excitation frequencies.

In this paper we present the experimental results on the structure, morphology, and spectroscopic properties and on the photocatalytic activity of ETS-4 and ETS-10, which are different types of microporous titanosilicates of different structure. The results obtained on titanosilicates are compared with data obtained on TiO_2 (P25), representing the classical Ti-based photocatalyst. The aim of this investigation is twofold: (a) to elucidate the role of surface structures in influencing the photocatalytic activity and selectivity and to bring new information on activities of internal and external sites; (b) to verify the effect of altering the excitation frequency and hence the ratio between the contribution of the band gap and charge-transfer mechanisms on the photocatalytic processes.

(13) Anderson, M. W.; Terasaki, O.; Ohsuna, T.; Philippou, A.; Mackay, S. P.; Ferreira, A.; Rocha, J.; Lidin, S. *Nature* **1994**, *367*, 347−351.
(14) Anderson, M. W.; Terasaki, O.; Ohsuna, T.; Malley, P. J. O.; Philippou, A.; Mackay, S. P.; Ferreira, A.; Rocha, J.; Lidin, S. *Philos. Mag. B* **1995**, *71*, 813−841.
(15) Borello, E.; Lamberti, C.; Bordiga, S.; Zecchina, A.; Otero Arean, C. *Appl. Phys. Lett.* **1997**, *71*, 2319−2321.
(16) Lamberti, C. *Microporous Mesoporous Mater.* **1999**, *30*, 155−163.
(17) Bordiga, S.; Palomino, G. T.; Zecchina, A.; Ranghino, G.; Giamello, E.; Lamberti, C. *J. Chem. Phys.* **2000**, *112*, 3859−3867.
(18) Damin, A.; Xamena, F. X. L.; Lamberti, C.; Civalleri, B.; Zicovich-Wilson, C. M.; Zecchina, A. *J. Phys. Chem. B* **2004**, *108*, 1328−1336.
(19) Howe, R. F.; Krisnandi, Y. K. *Chem. Commun.* **2001**, 1588−1589.
(20) Krisnandi, Y. K.; Southon, P. D.; Adesina, A. A.; Howe, R. F. *Int. J. Photoenergy* **2003**, *5*, 131−140.
(21) Liu, Y.; Dadap, J. I.; Zimdars, D.; Eisenthal, K. B. *J. Phys. Chem. B* **1999**, *103*, 2480−2486.
(22) Kim, S.; Choi, W. *J. Phys. Chem. B* **2005**, *109*, 5143−5149.

A brief description of the topics outlined in this work follows. The bulk and surface structure of both ETS-4 and ETS-10 titanosilicates is described in section 3 using volumetric measurements and SEM microscopy. Section 4 is devoted to the spectroscopic characterization of the two materials: UV−vis, Raman, and IR in subsections 4.1, 4.2, and 4.3, respectively. H_2O_2 and catechol molecules have been used to titrate the number of accessible titanols in subsection 5.1. The dimensional differences of the two probes allows us to discriminate between titanols present in the zeotypes channels and those present on the external surface of the microcrystals. Subsection 5.2 reports an UV−Vis characterization of the surface complexes formed by phenol (P), 4-chlorophenol (CP), 2,5-dichlorophenol (DCP), 2,4,5-trichlorophenol (TCP), 1,3,5-trihydroxybenzene (THB), and 2,3-dihydroxynaphthalene (DHN) molecules on ETS-4, ETS-10, and P25 solids. This study allowed us to determine the charge-transfer transition of the adsorbates that may result in the activation of the CT mechanism. Finally, section 6 reports the photocatalytic results on the degradation of CP, DCP, and TCP (subsection 6.1) and of P, THB, and DHN (subsection 6.2) on the three photocatalysts.

2. Experimental Section

Na-ETS-4 was prepared with the procedure reported by Kuznicki.[23] X-ray powder diffraction analysis, performed with a Philips PW 1830 diffractometer and with use of Cu Kα radiation, was performed to identify the product phase and to evaluate the crystallinity. The XRD pattern (not shown for sake of brevity) is in good agreement with the published ETS-4 data,[24] indicating the presence of a single phase. The ETS-10 sample, kindly supplied by Engelhard, comes from the same batch already used for previous investigations.[11,12,15−18,25−27] All the organic compounds phenol (P), 4-chlorophenol (CP), 2,5-dichlorophenol (DCP), 2,4,5-trichlorophenol (TCP), 1,3,5-trihydroxybenzene (THB), 2,3-dihydroxynaphthalene (DHN), and catechol were purchased from Aldrich and used as received. As for hydrogen peroxide, H_2O_2/H_2O solution (30 wt %) was used.

Adsorption measurements were performed with a Micromeritics ASAP 2010 sorption analyzer. Surface area was obtained by N_2 adsorption at 77 K on ETS-4 and ETS-10 previously outgassed at 400 and 500 K, respectively. Accessible microporous volume has been estimated from the t-plot (Harkins and Jura thickness equation) of the N_2 adsorption data.

The morphology and the dimension of the crystals were determined by scanning electron microscopy using a Leica Cambridge Stereoscan 420 instrument, equipped with an energy-dispersive X-ray spectrometer (EDS). The IR spectra, under a controlled atmosphere, were collected using a Bruker IFS66 spectrometer with a resolution of 2 cm^{-1}. The Raman spectra were recorded with a Renishaw micro-Raman system 1000 spectrometer equipped with a He−Cd laser emitting at $\lambda = 442$ nm (22625 cm^{-1}) or at $\lambda' = 325$ nm (30770 cm^{-1}), the output power of which was 25% of the maximum value. The photons scattered by the sample were dispersed by a 2400 lines/mm grating monochromator and simultaneously collected on a CCD camera.

The optical properties of surface complexes formed by interaction of Ti−OH groups with various adsorbates (H_2O_2, catechol, (poly)-chlorinated and (poly)hydroxylated aromatic compounds) have been studied by UV−Vis spectroscopy in the reflectance mode with a Perkin-Elmer Lambda 19 spectrometer in the 50000−4000 cm^{-1} range. Adsorbates have been dosed to the titanosilicate samples in aqueous solution for H_2O_2 and in CH_2Cl_2 solution for the remaining molecules. After contact, the solvent was eliminated by drying at RT. The UV−Vis spectra have so been obtained on the dry samples. This procedure is aimed to avoid systematic errors in the evaluation of the intensities of adsorbate-specific UV−Vis bands, as different fillings of the intracrystalline voids by the solvent molecules have an important effect on the scattering properties of the powder.[28] The concentration of the adsorbates on the dry samples was always exceeding the concentration of the surface Ti−OH sites by a factor of 10 at least.

For photocatalytic reactions, carried out at 308 K, the irradiation was carried out on 5 mL of aqueous suspension containing 1×10^{-4} M organic compounds and 0.1 g L^{-1} of catalyst, using a 1500 W xenon lamp (solarbox, CO.FO. MEGRA, Milan, Italy) simulating AM1 solar light. This lamp was equipped with a cutoff filter at 310 nm (32260 cm^{-1}) for UV experiments or a cutoff filter at 400 nm (25000 cm^{-1}) for the experiment in the visible region. The content of the cell was filtered through a 0.45 μm cellulose acetate filter (Millipore HA) and analyzed using high-performance liquid chromatography (HPLC). The wavelength used on the UV−Vis detector of the HPLC equipment was 220 nm. A Rheodyne injector, a RP C18 column (Lichrochart, Merck, 12.5 cm × 0.4 cm, 5 μm packing), a high-pressure two-pump gradient (Merck Hitachi L-6200 and L-6000 pumps), and UV−Vis detection (Merck Hitachi L-4200) were used ($\lambda = 220$ nm). Calibration of the equipment was done according to standard methods. The irradiation of the two equimolar mixtures of the three molecules (i.e., CP/DCP/TCP and P/THB/DHN) was done by using the same condition as before, and using global concentrations of 3.0×10^{-4} M.

3. Bulk and Surface Structure of ETS-4 and ETS-10

3.1. Bulk Structure of Ideal Crystals. The idealized framework structure of ETS-4 with formula $Na_6[Ti_3Si_8O_{25}]$ as deduced from ref 29 is represented in Figure 1a while that of the parent ETS-10 titanosilicate, ($Na_{11.6}K_{4.4}[Ti_8Si_{39}O_{104}]$), is reported in Figure 1b, according to the single-crystal XRD study of Wang and Jacobson.[30] As the charge-balancing cations (Na^+, K^+) do not play a primary role in determining the photocatalytic activity (associated with Ti centers), the cationic sites are omitted for simplicity in Figure 1.

Both 12- and 8-membered rings are present in the ETS-4 framework where the extraframework cations are mainly located. 12-membered rings, running along the *c* direction, are well visible in Figure 1a, while this does not hold for

(23) Kuznicki, S. M. U.S.Patent 438939, 1990.
(24) Nair, S.; Jeong, H. K.; Chandrasekaran, A.; Braunbarth, C. M.; Tsapatsis, M.; Kuznicki, S. M. *Chem. Mater.* **2001**, *13*, 4247−4254.
(25) Zecchina, A.; Arean, C. O.; Palomino, G. T.; Geobaldo, F.; Lamberti, C.; Spoto, G.; Bordiga, S. *Phys. Chem. Chem. Phys.* **1999**, *1*, 1649−1657.
(26) Xamena, F.; Damin, A.; Bordiga, S.; Zecchina, A. *Chem. Commun.* **2003**, 1514−1515.
(27) Prestipino, C.; Solari, P. L.; Larnberti, C. *J. Phys. Chem. B* **2005**, *109*, 13132−13137.
(28) Bonino, F.; Damin, A.; Ricchiardi, G.; Ricci, M.; Spano, G.; D′Aloisio, R.; Zecchina, A.; Lamberti, C.; Prestipino, C.; Bordiga, S. *J. Phys. Chem. B* **2004**, *108*, 3573−3583.
(29) Kuznicki, S. M.; Thrush, K. A.; Allen, F. M.; Levine, S. M.; Hamil, M. M.; Hayhurst, D. T.; Mansour, M. Synthesis and Adsorpitive Properties of Titanium Silicate Molecular Sieves. In *Synthesis of Microporous Materials*; Ocelli, M. L., Robson, H. E., Eds.; Van Nostrand Reinhold: New York, 1992; Vol. 1-Molecular sieves, p 427.
(30) Wang, X. Q.; Jacobson, A. J. *Chem. Commun.* **1999**, 973−974.

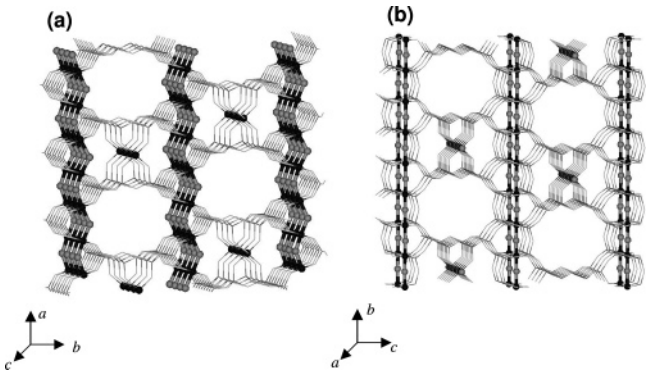

Figure 1. Joint sticks and sticks and balls representation of ETS-4 (part a) and ETS-10 (part b) structure viewed almost along the *c* and *a* axes, respectively. The whole structure is reported by stick representation, where the junction of four sticks represents a [SiO_4] unit. The sticks and balls representation has been used to underline the −O−Ti−O−Ti− wires (O, gray balls; Ti, dark balls). In part (a), also the isolated [TiO_5] units of ETS-4 can be appreciated (isolated dark balls). For simplicity we have arbitrarily assumed an ordered structure of [TiO_5] units occupying the 12-membered rings in a strictly alternated way, see text. For sake of clarity charge-balancing cations and water molecules (both structural and adsorbed) have been omitted. Note that to align the −O−Ti−O−Ti− zigzag wires of ETS-4 with one of the two linear one of ETS-10, two different crystal orientations have been used.

8-membered rings as they run along the *b* direction. Two types of Ti atoms are present in the ETS-4 structure forming [TiO_6] and [TiO_5] units.[29] The former are mutually connected along the *a* axis, forming zigzag −O−Ti−O−Ti− nanowires. In the perpendicular *bc* plane they exhibit four Ti−O−Si connections (Figure 1a). By analogy with ETS-10 it is expected that these chains can show quantum wire properties.[15−17] The latter are aligned along the *c* direction. Such [TiO_5] units can be considered as isolated as they are not directly connected via an oxygen bridge. Four out of the five first shell O atoms are framework oxygen atoms bridged with Si atoms in an almost C_{4v} local symmetry, the C_4 axis of which is parallel to the *c* axis of the crystal. The fifth first shell O atom belongs to a water molecule located on the C_4 axis in opposite position with respect to the first four. These H_2O molecules (not represented in Figure 1a for simplicity) are strongly adsorbed to the Ti atom and must be considered as structural water, as their removal, after prolonged evacuation (at $T > 450$ K), causes the structure collapse.

The structure of ETS-10 is formed by chains of corner-sharing [TiO_6] octahedra linked to each other by tetrahedral [SiO_4] units, generating 12-membered ring interconnected channels running along the *b* and *a* axes, the latter well visible in Figure 1b. Also visible are the −O−Ti−O−Ti− nanowires, running along the perpendicular *b* and *a* axes. In this case we are dealing with linear chains as both the O−Ti−O and the Ti−O−Ti angles are close to 180°.[18,27,30]

Actually, the structures of both ETS-4 and ETS-10, reported in Figure 1, are largely idealized as we are dealing with defective materials. This is particularly true for ETS-4 because, while the occupancy factor of the [TiO_6] units forming the zigzag −O−Ti−O−Ti− chains is 1, that of the isolated [TiO_5] units is smaller than unit, in the 0.5−0.24 range, depending on the refinement.[24,31,32] The same holds for the four silicon atoms representing the second shell environment of such pentacoordinated Ti. We shall label such larger units as [$H_2OTi(OSi)_4$]. For simplicity reasons, the situation depicted in Figure 1a corresponds to an occupancy of the [$H_2OTi(OSi)_4$] units equal to 0.5 and to the fact that the 12-membered rings are either fully occupied by [$H_2OTi(OSi)_4$] units or totally empty, in an ordered alternated way. On a graphical ground, this ordered structure allows a better understanding of the differences between [TiO_6] and [TiO_5] units, but has been rejected by Cruciani et al.,[31] owing to the absence of doubling of the *b*-axis in their synchrotron radiation powder XRD pattern. They proposed an alternative model consistent with the *Cmmm* superposition structure where the partial occupancy of the [$H_2OTi(OSi)_4$] units is explained by a statistical distribution of the empty 12-membered rings in the ETS-4 structure. This model implies a disordered stacking of layers, causing segmentation of the 12-membered channel system, and predicts a poor adsorption capability of the material. For a view of such, more complex situation the reader is referred to Figure 3 of Cruciani et al.'s work.[31]

Braunbarth et al.[32] have modeled the real structure of ETS-4 as a combination of four polymorphs. This causes the appearance of numerous stacking faults which have the effect of blocking the 12-membered rings channels which are consequently accessible to diffusing molecules for a limited length only.[33] Conversely, the 8-membered rings, running along the *b* direction, are not blocked by stacking faults. Also, this approach implies that on ETS-4 we deal only with 12-membered ring pockets located where the blocked channels emerge on the external surfaces and with narrow 8-membered rings partially occluded by the presence of charge-balancing Na^+ counterions and by the structural water molecules strongly bonded to the pentacoordinated Ti atoms.

As for ETS-10, two different polymorphs have been found.[13,14,34−36] In this case the defectivity is less pronounced than that for ETS-4.

3.2. Internal and External Surface Area: N_2 Adsorption/Desorption Isotherms. To verify the actual accessibility of the pores, we have performed N_2 adsorption/desorption isotherms at 77 K on ETS-4 and ETS-10 samples previously outgassed at 400 and 500 K, respectively (see Figure S1 of the Supporting Information). It has been found that ETS-10 shows a microporous structure, while ETS-4 does not. These data indicate that the defectivity degree of the real ETS-4 is sufficiently high to destroy the microporous nature of the ideal structure. As for ETS-10, the relatively lower degree of defectivity in combination with the presence of two interconnecting sets of large-pore channels guarantees the microporosity nature of the real material.

(31) Cruciani, G.; De Luca, P.; Nastro, A.; Pattison, P. *Microporous Mesoporous Mater.* **1998**, *21*, 143−153.
(32) Braunbarth, C.; Hillhouse, H. W.; Tsapatsis, M.; Burton, A.; Lobo, R. F.; Jacubinas, R. M.; Kuznicki, S. M. *Chem. Mater.* **2000**, *12*, 1857−1865.
(33) Marathe, R. P.; Farooq, S.; Srinivasan, M. P. *J. Phys. Chem. B* **2005**, *109*, 3257−3261.
(34) Anderson, M. W.; Agger, J. R.; Hanif, N.; Terasaki, O. *Microporous Mesoporous Mater.* **2001**, *48*, 1−9.
(35) Ohsuna, T.; Terasaki, O.; Watanabe, D.; Anderson, M. W.; Lidin, S. *Stud. Surf. Sci. Catal.* **1994**, *84*, 413−420.
(36) Southon, P. D.; Howe, R. F. *Chem. Mater.* **2002**, *14*, 4209−4218.

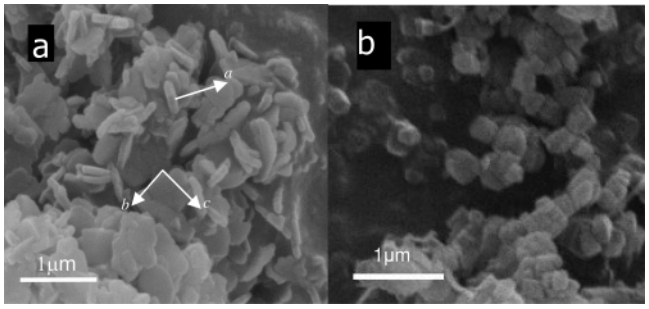

Figure 2. SEM micrographs of ETS-4 and ETS-10 materials: parts (a) and (b), respectively. For ETS-4, according to literature data,[37,38] reporting that $l_a \ll l_c < l_b$, it has been possible to identify the crystal orientations, which have been marked for two defined crystallites in part (a).

On a quantitative ground, the t-plot method was used to evaluate the external surface area which is 25 ± 2 m^2 g^{-1} on ETS-4 and 21 ± 2 m^2 g^{-1} on ETS-10, representing about one-third of that measured for the reference TiO_2 (P25) material. Accessible microporous volume was evaluated to be 328 m^2 g^{-1} on ETS-10 and only 10 m^2 g^{-1} on ETS-4, confirming what is immediately seen from Figure S1. The value of 10 m^2 g^{-1} found for ETS-4 represents the volume of the fraction of 12-membered ring channels starting from the crystal *ab* surface up to the first channel interruption by stacking faults (Figure 1 and related discussion). No mesopore presence has been observed on both samples.

3.3. Crystal Morphology: A SEM Investigation. SEM analysis of ETS-4 (Figure 2a) reveals agglomerates of uniform plates with size in the 200−500 nm range and ∼100 nm thickness, while ETS-10 is constituted by cubic-like microcrystals with edges in the 250−300 nm range (Figure 2b). These crystallites dimensions justify the external surface area value obtained by adsorption/desorption measurements. As far as ETS-4 is concerned, the relation between the morphology of the crystals and the crystallographic axes has been established on the basis of XRD and transmission electron microscopy (TEM) investigation by Braunbarth et al.:[37] the longest axes of the crystal and, therefore, the direction of the fastest growth, correspond to the crystallographic *b* axes, i.e., the direction where the −O−Ti−O−Ti− zigzag chains are running (Figure 1a). The relationship of the crystal lengths along the three directions is: $l_a \ll l_c < l_b$. The more recent study of Miraglia et al.[38] shows that the morphology of ETS-4 crystals strongly depends on the synthesis condition. When the synthesis results in plate-shaped crystals, the orientation of the axis previously reported by Braunbarth et al.[37] is confirmed. According to what found in those careful studies, it has been possible to identify the crystal orientations for some of the crystals reported in the SEM micrograph of Figure 2a.

The crystals morphology investigated by SEM plays a key role in our study as it governs the portioning of the external surface area among the exposed faces where the external Ti−OH groups are located. Owing to the defectivity of real ETS-4 crystals discussed above and according to the previous studies on ETS-10,[11,12] we conclude that the Ti−OH centers active in photocatalysis are those hosted at the external surface of both materials. As a consequence, in the next subsection, we will briefly discuss the surface morphology of both systems.

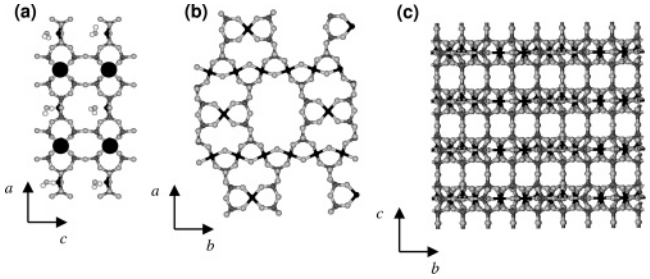

Figure 3. Sticks and balls representation of the *ac*, *ab*, and *cb* external surfaces of ETS-4 obtained by cutting the ideal tri-dimensional crystal reported in Figure 1a, parts (a), (b), and (c), respectively. Black, light gray, and dark gray balls refer to Ti, O, and Si atoms, respectively. External Ti−OH groups belonging to terminal −O−Ti−O−Ti− chains are evidenced by black circles and are present only on the *ac* faces, part (a). Structural water molecules adsorbed on [TiO_5] units can be visible in part (a) inside the 8-membered pores. Extraframework cations are not indicated for sake of clarity.

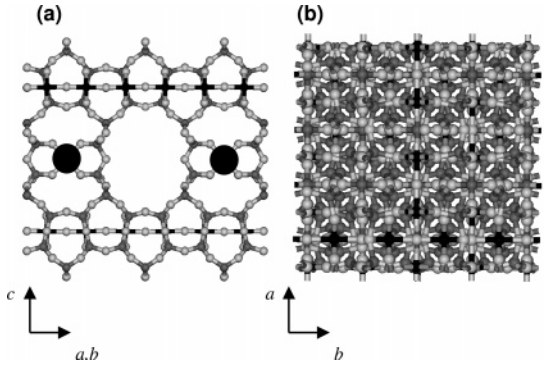

Figure 4. Sticks and balls representation of the *ac*, *bc* (part a), and *ab* (part b) external surfaces of ETS-10 obtained by cutting the ideal tri-dimensional crystal reported in Figure 1b. Black, light gray, and dark gray balls refer to Ti, O, and Si atoms, respectively. External Ti−OH groups belonging to terminal −O−Ti−O−Ti− chains are evidenced by big black circles and are present on *ac* and *bc* faces, part (a). Extraframework cations are not indicated for sake of clarity.

3.4. Surface Structure of Ideal ETS-4 and ETS-10 Crystals. A picture of the structure of the faces at the atomic level is represented in Figure 3 for ETS-4 and in Figure 4 for ETS-10. As for the structure of the most exposed faces of TiO_2 (anatase), used as comparison in the photocatalytic measurements, reference is made to the literature.[39−42] Note that the representations of Figure 3 and Figure 4 are certainly simplified since the real surfaces are stepped,[32,36] and consequently will be much more defective than those shown, and that the estimates of surface titanol concentrations made are very much on the low side. Defects can also be present on the internal walls of the 12-membered channels.

From a comparison between Figure 3 and Figure 4 it can be inferred that the situation of ETS-4 and ETS-10 is

(37) Braunbarth, C. M.; Boudreau, L. C.; Tsapatsis, M. *J. Membr. Sci.* **2000**, *174*, 31−42.
(38) Miraglia, P. Q.; Yilmaz, B.; Warzywoda, J.; Sacco, A. *J. Cryst. Growth* **2004**, *270*, 674−684.
(39) Zecchina, A.; Scarano, D.; Bordiga, S.; Spoto, G.; Lamberti, C., Surface structures of oxides and halides and their relationships to catalytic properties. In *Advances in Catalysis*; Academic Press Inc.: San Diego, CA, 2002; Vol. 46, pp 265−397.
(40) Cerrato, G.; Marchese, L.; Morterra, C. *Appl. Surf. Sci.* **1993**, *70−1*, 200−205.
(41) Morterra, C. *J. Chem. Soc., Faraday Trans 1* **1988**, *84*, 1617−1637.
(42) Diebold, U. *Surf. Sci. Rep.* **2003**, *48*, 53−229.

different. In fact, in ETS-4, the ziz-zag −O−Ti−O−Ti− chains are running along the *b* axis only and emerge on *ac* faces; see Figure 3a where they have been represented as full circles, indicating the presence of a surface titanol. From this view, we can appreciate the 8-membered channels not visible in Figure 1a. According to literature data[37,38] and to our SEM study (see Figure 2a), as the *ac* faces scarcely contribute to the external surface area (slightly more than 10%, corresponding to about 3 $m^2\ g^{-1}$), we are expecting a low number of such Ti−OH groups available for guest molecules per gram of ETS-4. As the concentration of titanols on this ideal face is about 1.4 nm^{-2}, we are dealing for ETS-4 with an estimated number of titanols of $4.2 \times 10^{18}\ g^{-1}$. Depending on the cutting planes parallel to the *ac* face, [TiO_5] groups may appear at the surface or not. This fact does not introduce any arbitrariness in the counting of the Ti−OH groups working in photocatalysis as such Ti−OH groups will be isolated by the siliceous matrix and cannot be reached by charge carriers.

A high number of titanol groups belonging to the terminal of the linear −O−Ti−O−Ti− chains is present per gram of ETS-10, as they are found on both *ba* and *bc* faces (Figure 4a). Owing to the cubic shape of ETS-10 crystals (Figure 2b), such faces represent $^2/_3$ of the external surface area, i.e., 14 $m^2\ g^{-1}$. Being the concentration of Ti−OH groups on both *ba* and *bc* faces is about 0.5 nm^{-2}, the estimated number of titanols is $7.0 \times 10^{18}\ g^{-1}$ for ETS-10.

On ETS-4 the faces perpendicular to the *c* direction, representing about 30% of the total surface area (Figure 2a), expose only the isolated Ti−OH generated from cutting a [TiO_5] unit; see Figure 3b where a 12-membered ring is well visible. As discussed above, such titanols are not photoactive as they are not connected with the conducting −O−Ti−O−Ti− wires.

The most extended face of ETS-4 (about 60% of the total surface area, see Figure 2a) are perpendicular to the *a* direction and parallel to the zigzag chains. No channel is emerging from this surface (Figure 3c). The same holds for the *ab* surface in ETS-10 (Figure 4b).

For the *ab* and *bc* surfaces in ETS-4 (Figure 3b and Figure 3c, respectively) and for the *ab* surface in ETS-10 (Figure 4b), different choices of the cutting planes are possible and their adoption is somewhat arbitrary. As all these faces are parallel to the −O−Ti−O−Ti− wires, the chosen cutting plane may uncover such wires, resulting in electrically connected surface Ti−OH groups, or may let the wires buried inside the siliceous matrix.

In conclusion, three types of Ti−OH groups are present on these idealized terminations: (a) photoactive Ti−OH terminating a −O−Ti−O−Ti−, more abundant on ETS-10 than on ETS-4; (b) isolated Ti−OH groups from surface [TiO_5] groups, present on ETS-4 only; (c) vicinal HO−Ti−O−Ti−OH groups present on both samples, presumably located at defects. It is finally worth underlining that when at the surface a second Ti−O−Si bridge is broken, geminal $Ti(OH)_2$ groups will appear.

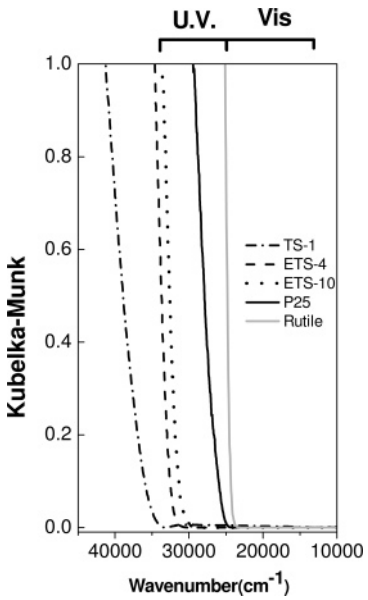

Figure 5. UV−Vis spectra of TS-1 (dot dashed curve), ETS-4 (dashed curve), ETS-10 (dotted curve), P25 (full black curve), and TiO_2 (bulk rutile, full gray curve), listed as a function of decreasing E_g. Also evidence on top of the figure is the frequency ranges used for the photocatalytic experiments under UV illumination up to 310 (32260 cm^{-1}) and under visible illumination 400 nm (25000 cm^{-1}), see section 6.

4. Spectroscopic Properties of ETS-4 and ETS-10

4.1. Band Gap Properties: A UV−Vis DRS Study. One of the most important physical parameters of a Ti-based photocatalyst is its band gap (E_g) as it determines the cutoff of the photons that can be used to produce an electron−hole pair according to the BG mechanism. The present paragraph is devoted to a brief description of the band gap properties of the investigated materials probed by UV−Vis DRS spectroscopy.

For both ETS-4 and ETS-10 titanosilicates, the presence of −O−Ti−O−Ti− chains strongly modifies the band gap value, as testified by spectra in the UV−Vis region (Figure 5). In fact, ETS-4 (dashed curve) and ETS-10 (dotted curve) show very similar absorption edges at about 33000−34000 cm^{-1}, which are assigned to valence to conduction band transitions in ziz-zag (ETS-4) (34000 cm^{-1}) and linear (ETS-10) (33000 cm^{-1}) quantum wires.[15−18,43] Due to the one-dimensional character of the −O−Ti−O−Ti− chains (quantum size effect), the absorption edges occur at a frequency higher than that in bulk TiO_2, occurring at 25600 and at 24400 cm^{-1} for anatase and rutile, respectively[44] (full gray curve for rutile). In comparison with ETS-10, the edge of ETS-4 occurs at a slightly higher frequency. This is probably related to a quantum effect associated with the shorter length of the −O−Ti−O−Ti−chains,[15] caused by the frequent interruptions (stacking faults). Of course, the absorbing properties of TiO_2 (absorption coefficient or cross section in the UV region) are definitely higher than those of ETS-4 and ETS-10 because the number of titanium chromophores is definitely larger.

(43) Krisnandi, Y. K.; Lachowski, E. E.; Howe, R. F. *Chem. Mater.* **2006**, *18*, 928−933.
(44) Sandroff, C. J.; Hwang, D. M.; Chung, W. M. *Phys. Rev. B* **1986**, *33*, 5953.

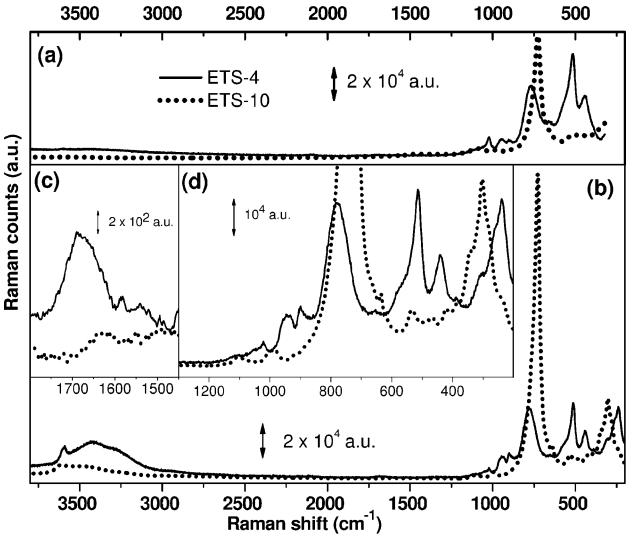

Figure 6. Raman spectra of ETS-4 (solid curves) and ETS-10 (dotted curves) titanosilicates exposed to the ambient atmosphere. Part (a) spectra collected using an excitation laser of $\lambda = 325$ nm. These spectra are recorded using a filter cutting at Raman shifts smaller than 320 cm^{-1}. Part (b) spectra collected using an excitation laser of $\lambda = 442$ nm. Parts (c) and (d) report a magnification of the spectra of part (b) in the region of H_2O bending and framework stretching modes, respectively.

As for P25, owing to the small crystal size, a slight but well measurable blue shift of the edge is observed with respect to rutile (Figure 5). Of course, all these edges occur at definitely lower frequency than the absorption of isolated Ti centers in titanium silicalite-1 (TS-1), behaving as an isolated [TiO_4] quantum dot.[15,28,45−47]

The set of these solids affords a group of photosystems characterized by a large spread of the band gap and thus responding to photons of different frequencies. The progressive blue shift of the E_g is associated with the evolution from a single site transition, [TiO_4] unit in TS-1, to transitions associated with linear −O−Ti−O−Ti− chains of increasing average length (ETS-4 and ETS-10) to transitions associated with a tri-dimensional frameworks of high surface area (P25) and bulk (rutile) nature. Notice that transitions associated with small clusters either entrapped in the zeolite nanocavities[48] or as part of a framework[49−51] are reported to be intermediate between those of isolated Ti sites and those of TiO_2.

4.2. Investigation of Framework Stretching Modes by Raman. The Raman spectra of ETS-4 and ETS-10 exposed to the ambient atmosphere are compared in Figure 6. Based on our experience, the heating power of the laser beam causes a partial water desorption from the channels of zeolite and zeotype materials. Reported spectra are thus referring to partially dehydrated systems. Parts (a) and (b) of the figure report the whole spectra collected with an excitation source of $\lambda = 325$ and 442 nm, respectively. The Raman spectra of both samples exhibit the main modes already reported in the literature.[18,36,52−54]

The Raman spectrum of ETS-10, collected with both wavelengths, is dominated by the strong mode at 725 cm^{-1}, assigned by Damin et al.[18] to a collective (totally symmetric) stretching mode involving the −O−Ti−O−Ti− chains. A second rather strong, but much more broad, component is observed at 305 cm^{-1}, while several minor components are present in the 1150−400 cm^{-1} range, being much better resolved when $\lambda = 442$ nm is used; see the magnification reported in Figure 6d. A detailed assignment of the ETS-10 vibrational modes has been reported elsewhere.[18]

Coming to ETS-4, the total symmetric stretching mode involving the −O−Ti−O−Ti− chains is observed at 780 or 770 cm^{-1} depending on whether the $\lambda = 442$ nm or the $\lambda' = 325$ nm excitation source is used. Note also that the adopted laser affects its relative intensity, with respect to the other main modes of ETS-4. Whatever is the excitation source, this mode is definitively blue-shifted, broader and less intense than that of the analogous one observed in ETS-10. These differences may be due to the different abundance of the chains, the different structure (zigzag for ETS-4 and linear for ETS-10), and the average length (certainly shorter on ETS-4 which is a very defective material). ETS-4 shows absorptions in the 990−950 and 550−450 cm^{-1} ranges that are absent or very weak on ETS-10. In particular, the modes at 514, 441, and 240 cm^{-1} are as strong as the chain mode (Figure 6d). We tentatively assign them to modes associated with the stretching and bending of SiOTi groups involving isolated 5-fold coordinated Ti centers (i.e., those carrying the structural water molecule, see section 3.1.). Comparison with the Raman spectrum of $CsTiSi_2O_{6.5}$ silicotitanate, which contain 5-fold coordinated Ti centers, is in agreement with this assignment.[53]

It is finally worth noticing that in this work we report, for the first time, Raman spectra of ETS-4 and ETS-10 recorded with two different excitation sources. This allows us to be differently sensitive to different vibrational modes. Fine differences have been observed for the framework modes of the two structures; however, the more striking difference between the two set of spectra concerns the modes of the adsorbed water molecules. The spectra collected with $\lambda' = 325$ nm (Figure 6a) do not show any appreciable vibrational feature due to adsorbed water. This is not surprising as the H_2O molecule is a very weak Raman scatterer. This is the reason, from the purely spectroscopic point of view, the spectra reported in Figure 6b ($\lambda = 442$ nm) are remarkable. In both cases the typical broad ν(O−H) component of H_2O molecules hosted in zeolitic cages, usually observed in the IR spectra (vide infra subsection 4.3), is clearly visible in

(45) Bordiga, S.; Coluccia, S.; Lamberti, C.; Marchese, L.; Zecchina, A.; Boscherini, F.; Buffa, F.; Genoni, F.; Leofanti, G.; Petrini, G.; Vlaic, G. *J. Phys. Chem.* **1994**, *98*, 4125−4132.
(46) Lamberti, C.; Bordiga, S.; Arduino, D.; Zecchina, A.; Geobaldo, F.; Spanò, G.; Genoni, F.; Petrini, G.; Carati, A.; Villain, F.; Vlaic, G. *J. Phys. Chem. B* **1998**, *102*, 6382−6390.
(47) Ricchiardi, G.; Damin, A.; Bordiga, S.; Lamberti, C.; Spanò, G.; Rivetti, F.; Zecchina, A. *J. Am. Chem. Soc.* **2001**, *123*, 11409−11419.
(48) Corrent, S.; Cosa, G.; Scaiano, J. C.; Galletero, M. S.; Alvaro, M.; Garcia, H. *Chem. Mater.* **2001**, *13*, 715−722.
(49) Behrens, E. A.; Poojary, D. M.; Clearfield, A. *Chem. Mater.* **1996**, *8*, 1236−1244.
(50) Behrens, E. A.; Poojary, D. M.; Clearfield, A. *Chem. Mater.* **1998**, *10*, 959−967.
(51) Rocha, J.; Anderson, M. W. *Eur. J. Inorg. Chem.* **2000**, 801−818.
(52) Mihailova, B.; Valtchev, V.; Mintova, S.; Konstantinov, L. *Zeolites* **1996**, *16*, 22−24.
(53) Su, Y.; Balmer, M. L.; Bunker, B. C. *J. Phys. Chem. B* **2000**, *104*, 8160−8169.
(54) Armaroli, T.; Busca, G.; Milella, F.; Bregani, F.; Toledo, G. P.; Nastro, A.; De Luca, P.; Bagnasco, G.; Turco, M. *J. Mater. Chem.* **2000**, *10*, 1699−1705.

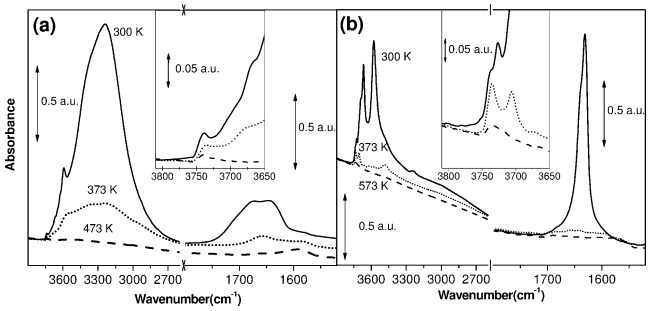

Figure 7. FTIR spectra of ETS-4 (part a) and ETS-10 (part b) upon dehydration at increasing temperatures. Left and right parts refer to the stretching and bending region of the water molecule, respectively. For both titanosilicates, the inset reports a magnification of the high-frequency region of the ν(O−H) components, where well-defined features can be appreciated. Solid (dotted) spectra are referred to samples activated at 300 K (373 K), while dashed spectra refer to samples activated at higher temperatures: 473 K for ETS-4 and 573 K for ETS-10.

the 3700−3000 cm^{-1} region. On ETS-4 we are even dealing with a well-defined component at 3600 cm^{-1} and with two structured shoulders at 3420 and 3270 cm^{-1}. With a sufficient scale enlargement (Figure 6c) also the correspondent bending mode around 1675 cm^{-1} is visible. This manifestation is definitely more intense on ETS-4 (full curve) than on ETS-10 (dotted curve), in agreement with the presence of structural water adsorbed on 5-fold coordinated Ti sites; see section 3.1 and Figure 3a. This demonstrates that the use of selected excitation lines can make Raman spectroscopy a useful tool for surface investigations.[47,55−59]

4.3. Vibrational Properties of Adsorbed H_2O Molecules and of TiOH and SiOH Groups: A FTIR Study. Besides the remarkable observation done with Raman spectroscopy, IR spectroscopy is the most useful technique to investigate the hydration level of a microporous material.[60] With the aim of confirming the different difficulties in eliminating water from ETS-4 and ETS-10 microporous titanosilicates, we have performed an FTIR investigation of both samples upon dehydration at increasing temperatures (Figure 7).

After prolonged (about 20 min) outgassing at 300 K (Figure 7a) the IR spectrum ETS-4, in the ν(O−H) stretching region, is characterized by two well-resolved components at 3740 cm^{-1} (see inset) and 3590 cm^{-1}, and by the presence of a broad, complex, and ill-defined band centered at 3230 cm^{-1}, with a clear high-frequency shoulder, extending down to 2900 cm^{-1}. In the water bending region the spectrum results in a broad absorption in 1690−1630 cm^{-1} range that well mirrors the component already observed with Raman (Figure 6c). These are the spectroscopic manifestations of water adsorbed on both Na^+ cations and to 5-fold coordinated Ti centers. The important red shift of the dominant mode at 3230 cm^{-1} testifies to the presence of strong H-bonding.[61] Activation at 373 K (dotted spectrum) results in a strong reduction of IR manifestation, owing to the desorption of most of the water adsorbed on Na^+ cations. The partial removal of adsorbed water makes slightly better defined the high-frequency region of the stretching modes, where the contribution of surface Ti−OH modes is expected. A detailed assignment is however not feasible owing to the simultaneous presence of surface Si−OH groups that are almost indistinguishable on a vibrational ground. An almost complete removal of water is obtained upon activation at 473 K (dashed spectrum), but this phenomenon is associated with a considerable loss of crystallinity, as confirmed by XRD analysis (pattern not reported for brevity, see ref 62 where the ETS-4 dehydration has been followed by XRD). The present IR study confirms the fundamental role of water adsorbed on the 5-fold coordinated Ti site of ETS-4 in preventing the structure collapse.

The IR spectrum of ETS-10 activated at 300 K is characterized by three peculiar and well-defined stretching components at 3726 (w, see inset), 3668 (vs, with a shoulder at 3690 cm^{-1}), and 3580 (vs) cm^{-1} and by a narrow bending mode at 1630 cm^{-1} (vs); see Figure 7b. The singularity of the two strong bands at 3668 and 3580 cm^{-1} consists of the small fwhm (≈15 and 40 cm^{-1}, respectively), indicating that we are dealing with water molecules, the vibrational properties of which are perfectly well ordered. This is totally unusual for weakly bonded H_2O molecules inside the zeolite channels[60] (the analogous band observed for ETS-4 has a fwhm of 400 cm^{-1}) and is more similar to the spectroscopic feature of a structurally well-defined Si−(OH)−Al Brønsted site inside a crystalline zeolitic framework.[61,63−65] This assignment can however not be done in the case of ETS-10 because the OH groups responsible for the components at 3726, 3668, and 1630 cm^{-1} are almost completely removed upon a mild outgassing treatment at 373 K and thus belong to physisorbed water molecules. This spectrum is characterized by two weak, but well-resolved peaks at 3735 cm^{-1} and at 3705 cm^{-1} (see inset in Figure 7b), corresponding to silanols and titanols (both external and internal) not involved in hydrogen bonding. Another very weak feature is also observed at 3488 cm^{-1}, attributed by Southon and Howe[36] to the ν(OH) of titanols located at internal defects sites (where the −O−Ti−O−Ti− chains are interrupted).

The parallel dehydration experiment followed by FTIR on P25 has been reported in Figure S2 of the Supporting Information.

(55) Bordiga, S.; Damin, A.; Bonino, F.; Ricchiardi, G.; Lamberti, C.; Zecchina, A. *Angew. Chem., Int. Ed.* **2002**, *41*, 4734−4737.
(56) Bordiga, S.; Damin, A.; Bonino, F.; Ricchiardi, G.; Zecchina, A.; Tagliapietra, R.; Lamberti, C. *Phys. Chem. Chem. Phys.* **2003**, *5*, 4390−4393.
(57) Bordiga, S.; Lamberti, C.; Ricchiardi, G.; Regli, L.; Bonino, F.; Damin, A.; Lillerud, K. P.; Bjorgen, M.; Zecchina, A. *Chem. Commun.* **2004**, 2300−2301.
(58) Groppo, E.; Lamberti, C.; Bordiga, S.; Spoto, G.; Zecchina, A. *Chem. Rev.* **2005**, *105*, 115−183 and references therein.
(59) Prestipino, C.; Regli, L.; Vitillo, J. G.; Bonino, F.; Damin, A.; Lamberti, C.; Zecchina, A.; Solari, P. L.; Kongshaug, K. O.; Bordiga, S. *Chem. Mater.* **2006**, *18*, 1337−1346.
(60) Bordiga, S.; Damin, A.; Bonino, F.; Zecchina, A.; Spanò, G.; Rivetti, F.; Bolis, V.; Lamberti, C. *J. Phys. Chem. B* **2002**, *106*, 9892−9905.
(61) Paze, C.; Bordiga, S.; Lamberti, C.; Salvalaggio, M.; Zecchina, A.; Bellussi, G. *J. Phys. Chem. B* **1997**, *101*, 4740−4751.
(62) Naderi, M.; Anderson, M. W. *Zeolites* **1996**, *17*, 437−443.
(63) Zecchina, A.; Xamena, F.; Paze, C.; Palomino, G. T.; Bordiga, S.; Arean, C. O. *Phys. Chem. Chem. Phys.* **2001**, *3*, 1228−1231.
(64) Regli, L.; Zecchina, A.; Vitillo, J. G.; Cocina, D.; Spoto, G.; Lamberti, C.; Lillerud, K. P.; Olsbye, U.; Bordiga, S. *Phys. Chem. Chem. Phys.* **2005**, *7*, 3197−3203.
(65) Zecchina, A.; Bordiga, S.; Vitillo, J. G.; Ricchiardi, G.; Lamberti, C.; Spoto, G.; Bjorgen, M.; Lillerud, K. P. *J. Am. Chem. Soc.* **2005**, *127*, 6361−6366.

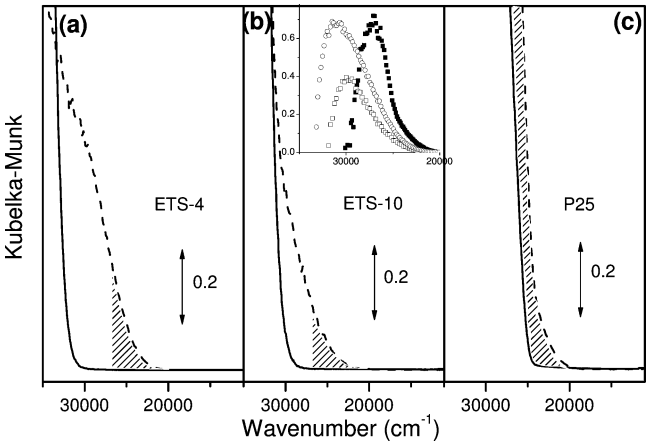

Figure 8. UV−Vis spectra of ETS-4, ETS-10, and P25 before (full lines) and after (dashed lines) interaction with H_2O_2/H_2O, parts (a), (b), and (c), respectively. In each part, the dashed areas represent the areas between the two curves in the 20000−27000 cm^{-1} range, which has been used to evaluate the relative number of titanols on the three samples, see text. Inset: difference spectra between the three materials before and after H_2O_2/H_2O contact for P25 (scattered full squares), ETS-10 (scattered empty square), and ETS-4 (scattered empty circle).

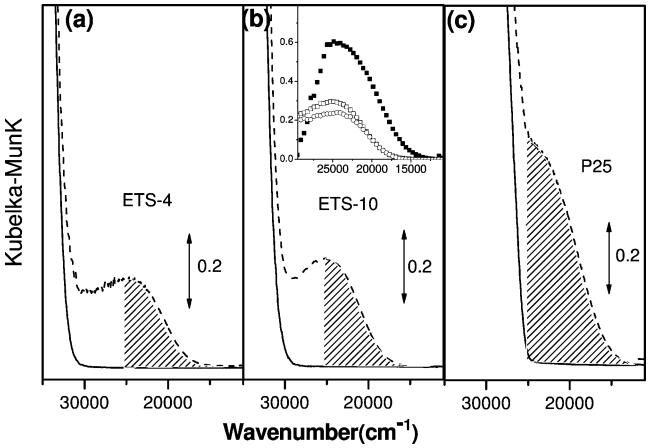

Figure 9. As Figure 8 for the interaction with cathecol.

5. UV−Vis Characterization of Surface Complexes Formed on ETS-4, ETS-10, and P25

UV−Vis spectroscopy has been used first (subsection 5.1) to titrate both total and surface titanols available on the catalyst surface, using hydrogen peroxide and catechol molecules, respectively. This part complements the surface morphology discussion reported in section 3. In subsection 5.2 we report the UV−Vis spectra of the aromatic molecules investigated in the photocatalytic study (section 6) in order to understand how the interaction with adsorbates modifies the photon absorbing properties of the system and to verify the possibility of opening the channel of the CT mechanism.

5.1. Titration of TiOH Groups with H_2O_2 and Catechol. As already documented by Xamena et al.,[12] accessible titanols (on internal and external surfaces) can be spectroscopically titrated with hydrogen peroxide because the formation of TiOOH complexes result in the appearance of a new LMCT at an energy lower than the band gap, conferring to the sample the typical yellow color.[12,28,55,66,67] On this basis, hydrogen peroxide could be considered as a probe of the amount of titanols accessible to small molecules, especially when excess H_2O_2 is used (as we did in the experiments reported below). The UV−Vis spectra of ETS-4, ETS-10, and P25 before and after interaction with H_2O_2/H_2O are illustrated in Figure 8.

On both ETS-4 and ETS-10, the clear absorption of the TiOOH groups is well-observable in the 32000−20000 cm^{-1} range. In principle, the ratio between the number of titanols present on the two samples can be deduced from the integrated area of the specific TiOOH band (A_{ETS-10}/A_{ETS-4}). In the present cases, the application of this method is not straightforward as the TiOOH-specific band is not well-defined in the spectra reported in Figure 8, as it is partially overshadowed by the band due to the E_g of the materials. This problem is particularly severe for the P25 sample, part (c). Assuming that the formation of TiOOH groups does not affect significantly the E_g of the material, difference spectra (see inset in Figure 8) allows one to single out the TiOOH-specific band. Performing the integration of the difference spectra from 20000 cm^{-1} to $\tilde{\nu}_{max}$ ($\tilde{\nu}_{max}$ = 32000, 29600, or 27000 cm^{-1}), we obtain a value of A_{ETS-10}/A_{ETS-4} ranging between 0.525 and 0.608. Taking into account the intrinsic limitations of the adopted method, we can more prudently consider that on ETS-4 we have about twice the number of titanol present on ETS-10. These data seem apparently to be in contrast with the number of titanols calculated in subsection 3.4 considering only the external surface and assuming an ideal defect-free crystal of the two materials: 4.2×10^{18} and 7.0×10^{18} titanols g^{-1} for ETS-4 and ETS-10, respectively. We can explain the titration results, considering the small size of H_2O_2, which is able to diffuse into the ETS-4 framework (for instance, via the 8-memberd rings which are not interrupted by the stacking faults), and titrate, not only the external titanols but also those located at internal defects (certainly abundant because of the defective character of ETS-4).

To verify the correctness of this explanation, a second set of titration experiments has been performed using catechol (1,2-dihydroxybenzene) as the probing molecule. As this aromatic molecule is certainly not able to penetrate inside the pores, the intensity of the LMCT band due to phenate adducts may be ascribed to external surface titanols only. It is well-known that catechol forms very stable complexes with titanol groups,[68] characterized by two peaks at 25000 and 35000 cm^{-1}.[69] The UV−Vis spectra of ETS-4, ETS-10, and P25 before and after interaction with catechol are illustrated in Figure 9. As for Figure 8, the inset shows the difference spectra.

From the reported spectra, it is evident that whereas the band at 35000 cm^{-1} cannot be observed as overshadowed by the E_g transition, the band at 25000 cm^{-1} is much better defined than that of TiOOH band reported in Figure 8 for

(66) Geobaldo, F.; Bordiga, S.; Zecchina, A.; Giamello, E.; Leofanti, G.; Petrini, G. *Catal. Lett.* **1992**, *16*, 109−115.
(67) Tozzola, G.; Mantegazza, M. A.; Ranghino, G.; Petrini, G.; Bordiga, S.; Ricchiardi, G.; Lamberti, C.; Zulian, R.; Zecchina, A. *J. Catal.* **1998**, *179*, 64−71.
(68) Moser, J.; Punchihewa, S.; Infelta, P. P.; Gratzel, M. *Langmuir* **1991**, *7*, 3012−3018.
(69) Borgias, B. A.; Cooper, S. R.; Koh, Y. B.; Raymond, K. N. *Inorg. Chem.* **1984**, *23*, 1009−1016.

the complex formed with H_2O_2. When the integration of the difference spectra from 12000 cm^{-1} to $\tilde{\nu}_{max}$ ($\tilde{\nu}_{max} = 30000$ or 25000 cm^{-1}) is performed, a value of A_{ETS-10}/A_{ETS-4} greater than unit (1.18 and 1.16, respectively) is obtained, qualitatively confirming the larger number of surface titanols expected for ETS-10; see section 3.4.

In the titration experiments performed on P25 catalyst (Figure 8c and Figure 9c), although the method of the difference spectra is much more critical owing to the severe overlap with the bulk E_g absorption, a much higher density of both TiOOH and phenates complexes is observed. This is not unexpected because for P25 we are dealing with a surface area of 60 $m^2\ g^{-1}$ covered by titanols groups. A value of A_{P25}/A_{ETS-4} around 2 and 3 is measured for TiOOH and phenates complexes, respectively. For the reason outlined above, these values have a qualitative character only.

5.2. Molecules Directly Involved in Photodegradation Experiments: (Poly)chlorinated and (Poly)hydroxylated Aromatic Compounds. To understand the excitation processes operating in the photocatalyst/pollutant-molecule system upon irradiating with photons of different energies, we have performed an UV−Vis study of the three catalysts interacting with (poly)chlorinated and (poly)hydroxylated aromatic compounds.

The importance of this spectroscopic investigation is related to the fact that the aromatic molecules forming surface complexes with titanol groups undergo a deep modification of their electronic structure, resulting in a significant red shift of their electronic transitions (HOMO → LUMO) that usually occur at energies lower than E_g. This opens a new route for the creation of charge carriers in the solid, when there is a suitable energy band match between the LUMO level of the adsorbed molecule and the conduction band of the solid (top left part of Figure 10: complex A). In that case, the adsorbed molecule can be excited with a photon of energy $h\omega$ (usually $<E_g$), promoting directly (or indirectly) an electron into the LUMO level, which can be successively transferred into the conduction band of the solid.[21,22,70−72] The same does not hold for the band alignment reported for complex B (top right part of Figure 10). Please note that both E_{LUMO} and E_{HOMO} values, of a given molecule, are modified by the solvent and by the interaction with the surface adsorption site. The values drawn in Figure 10 refer to the adsorbed molecule in the presence of the solvent (H_2O in our case). As a conclusion, for complex A, we are dealing with a CT from the adsorbed molecule to the solid, resulting in photooxidation of the molecule and to its consequent possible degradation (bottom left part of Figure 10). We shall refer to this alternative route for the photodegradation as the "CT mechanism", in contrast with the standard BG mechanism[73] (bottom right part of Figure 10); see also the Introduction.

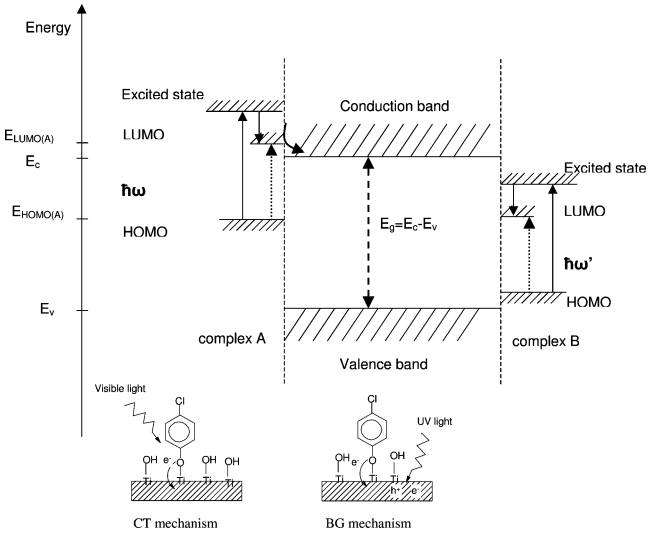

Figure 10. Top: Schematic representation of two different alignments between the conduction and valence bands of a semiconductor (middle) and the HOMO/LUMO levels of an adsorbed molecule (left and right). The band alignment reported for the surface complex A (left) allows an easy electron transfer from the LUMO (occupied upon $\hbar\omega$ irradiation) to the conduction band of the solid. The same does not hold for the band alignment reported for the surface complex B (right). For simplicity only the energy levels (E_{HOMO} and E_{LUMO}) of the A molecule are reported on the energy scale in the left part of the figure. When the excitation energy E is included in the $\hbar\omega < E < E_g$, only the CT mechanism may be operative; conversely, when $E > E_g$, also the BG mechanism is working. Bottom: schematic representation of a possible path for the CT and BG mechanisms left and right parts, respectively. The schemes have been drawn for the CP molecule. Note that the efficiency of the two processes may differ even by order of magnitudes.

On an experimental ground we just know the differences $E_{LUMO} - E_{HOMO} = \hbar\omega$ or $E_c - E_v = E_g$, E_c and E_v being the bottom of the conduction band and the top of the valence band, respectively. It is extremely complex to locate, in an absolute energy scale, the relative position of these levels using either experimental or theoretical approaches. The problem of the band alignment of two different systems (a semiconductor and a molecule in our case) is analogous to that of the definitions of the valence and conduction band lineups at semiconductor heterojunctions, largely debated in solid-state physics, because there is no intrinsic (absolute) energy scale to which energies are referred.[74−80] This inability to easily predict the correct band alignment is critical because the relative position of E_{LUMO} and E_c plays a tremendous role in establishing the efficiency of the CT mechanism. It is resonant when $E_{LUMO} \approx E_c$, becoming highly improbable when E_c exceeds E_{LUMO}, even just by few kT (complex B). On the opposite side, when $E_{LUMO} > E_c$ it is still very efficient, starting to decline only when $E_{LUMO} \gg E_c$. The main difference in the two mechanisms consists of the fact that the BG one offers to all molecules adsorbed on the surface almost the same chance to be degraded, while the

(70) Serpone, N.; Lawless, D.; Khairutdinov, R.; Pelizzetti, E. *J. Phys. Chem.* **1995**, *99*, 16655−16661.
(71) Rego, L. G. C.; Batista, V. S. *J. Am. Chem. Soc.* **2003**, *125*, 7989−7997.
(72) Lana-Villarreal, T.; Rodes, A.; Perez, J. M.; Gomez, R. *J. Am. Chem. Soc.* **2005**, *127*, 12601−12611.
(73) Minero, C.; Maurino, V.; Pelizzetti, E. Mechanism of the photocatalytic transformation of organic compounds. In *Semiconductor photochemistry and photophysics (Molecular and supramolecular photochemistry)*; Marcel Dekker: New York, 2003; Vol. 10, p 384.
(74) Van de Walle, C. G.; Martin, R. M. *Phys. Rev. B* **1986**, *34*, 5621−5634.
(75) Van de Walle, C. G.; Martin, R. M. *Phys. Rev. B* **1987**, *35*, 8154−8165.
(76) Bastard, G.; Brum, J. A.; Ferreira, R. *Solid State Phys.: Adv. Res. Appl.* **1991**, *44*, 229−415.
(77) Franciosi, A.; Van de Walle, C. G. *Surf. Sci. Rep.* **1996**, *25*, 1−140.
(78) Margaritondo, G. *Rep. Prog. Phys.* **1999**, *62*, 765−808.
(79) Lamberti, C. *Comput. Phys. Commun.* **1996**, *93*, 53−81. Lamberti, C. *Comput. Phys. Commun*. **1996**, *93*, 82−119.
(80) Lamberti, C. *Surf. Sci. Rep.* **2004**, *53*, 1−197.

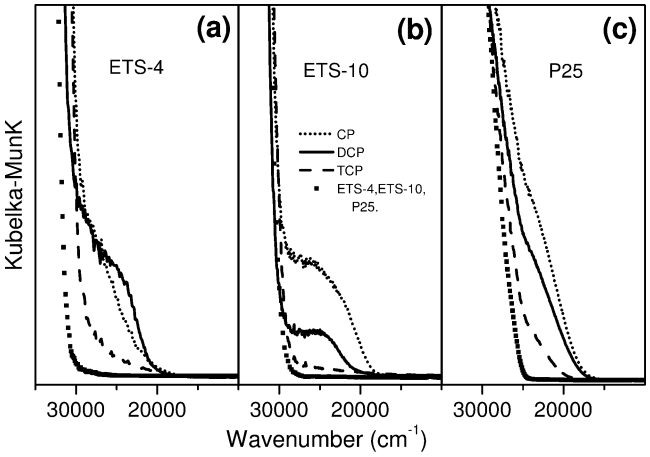

Figure 11. UV−Vis spectra of ETS-4 (part a), ETS-10 (part b), and P25 (part c) before (scattered square lines) and after interaction with CP (dotted curve), DCP (full black curve), and TCP (dashed curve).

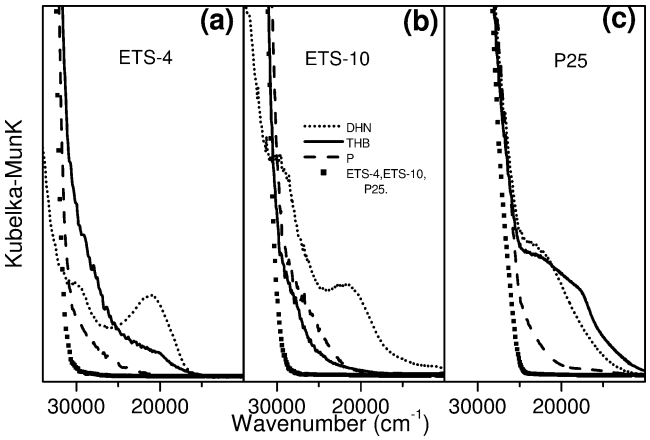

Figure 12. UV−Vis spectra of ETS-4 (part a), ETS-10 (part b), and P25 B (part c) before (scattered square curves) and after interaction with P (dashed curve), DHN (dotted curve), and THB (full black curve).

CT one is molecule-selective according to the closest match of the corresponding E_{LUMO} with the E_c of the hosting solid. Both mechanisms can be switched off by reducing the energy of the incoming photon below the corresponding threshold: $E_c - E_v = E_g$ or $E_{LUMO} - E_{HOMO} = \hbar\omega$, for the BG or the CT mechanism, respectively.

Coming to the spectroscopy of the adsorbed complexes, see Figure 11 and Figure 12 for the (poly)chlorinated and (poly)hydroxylated aromatic compounds, respectively, we will focus our attention on the position of the HOMO → LUMO transitions of the different adsorbed molecules only, without considering the band intensities as the spectra have been multiplied by arbitrary factors to allow a better graphical output when plotted together. By looking to the position of the HOMO → LUMO bands of the molecules in solution, see Table 1, we see that the adsorption on the titanol sites causes a remarkable red shift, reflecting an important electronic rearrangement. This rearrangement is the consequence of an important mixing between the molecular orbitals of the adsorbate and those of the solid surface: a fact that favors electron or holes transfer from the two systems. The spectroscopic features of these surface complexes will be commented on in section 6 when relevant for the discussion of the photocatalytic activity.

Table 1. Frequencies (cm^{-1}) of the Lowest Electronic Transition Observed in the UV−Vis Spectra of the (Poly)chlorinated and (Poly)hydroxylated Aromatic Compounds Adsorbed on ETS-4, ETS-10, and P25 Compounds; See Figures 11 and 12[a]

molecule	aq. solution	ETS-4	ETS-10	P25
CP	35500 (B)	26000 (T)	23000 (S)	21000 (S)
DCP	35400 (B)	24000 (S)	25000 (B)	23000 (S)
TCP	34400 (B)	28000 (T)	27000 (T)	24000 (T)
P	37000 (B)	28000 (T)	26000 (T)	24000 (T)
DHN	30400 (B)	21000 (B)-30000 (S)	21000 (B)-30000 (S)	23000 (S)
THB	37600 (B)	27000 (T)	28000 (T)	18000 (S)

[a] For comparison also the electronic transitions observed for the same molecules in aqueous solution (spectra not reported for brevity) are added. B = band; S = shoulder; T = tail.

Table 2. Photodegradation Rates for an Equimolar Mixture of CP, DCP, and TCP on ETS-4, ETS-10, and P25 (UV Irradiation Light)[a]

	rate ($M \times 10^5$ min^{-1})		
catalyst	ETS-4	ETS-10[b]	P25[b]
CP	0.002 (bg − ISS)	0.14 (bg + ct − ISS)	2.87 (BG)
DCP	0.23 (bg + CT)	0.20 (bg + CT)	2.78 (BG)
TCP	0.54 (bg + CT)	0.54 (bg + CT)	2.71 (BG)

[a] In parentheses is reported the degradation mechanism operating: BG = band gap, CT = charge transfer. When small letters are used (bg or ct), the mechanism is supposed to be present but with a low efficiency. When the inverse shape selectivity prevents the photodegradation, label ISS is added. [b] Values from ref 12.

6. Photocatalytic Results

6.1. Competitive Photodegradation of (Poly)chlorinated Aromatic Compounds. The results of the experiment about the competitive degradation rate of three chlorophenols (i.e., CP, DCP, and TCP) on ETS-10, ETS-4, and P25, obtained by using UV exciting frequencies, are reported in Table 2. Visible light is also slightly effective in photodegradation as already documented by several groups.[22,81−83] Consequently, corresponding results are not described here.

From these results is clear that P25 shows the highest degradation efficiency. CP degradation is 20 times smaller on ETS-10 than in P25 and is negligible on ETS-4. The degradation of DCP (TCP) on both ETS-10 and ETS-4 is about 10 (5) times lower than that on P25. Comparing the two zeolitic systems, the photodegradation activities are substantially similar. The much higher activity of P25 can be easily explained by the much higher number of available surface TiOH groups (see section 3 and subsection 5.1) and by the fact that all the photons of the UV lamp are able to activate the BG mechanism for P25 (see Figure 5 and Figure 10). For ETS-10 and ETS-4 only the high-energy photons have an $\hbar\omega$ higher than E_g. Conversely, the excitation light is perfectly able to promote a HOMO → LUMO transition for all three molecules on both ETS-10 and ETS-4 systems; see Figure 11. This means that photodegradation can occur, via the CT mechanism, for the adsorbates showing a band alignment similar to that of complex A in Figure 10.

P25 exhibits an almost null selectivity, being able to degrade the three molecules at nearly the same rate. This means that the main mechanism working on P25, upon

(81) Agrios, A. G.; Gray, K. A.; Weitz, E. *Langmuir* **2003**, *19*, 5178−5178.
(82) Agrios, A. G.; Gray, K. A.; Weitz, E. *Langmuir* **2004**, *20*, 5911−5917.
(83) Hurum, D. C.; Gray, K. A.; Rajh, T.; Thurnauer, M. C. *J. Phys. Chem. B* **2004**, *108*, 16483−16487.

Table 3. Photodegradation Rates for an Equimolar Mixture of P, THB, and DHN on ETS-4, ETS-10, and P25 (UV, λ > 310 nm, and Visible, λ > 400 nm, Irradiation Light)[a]

	rate ($M \times 10^5$ min^{-1})					
catalyst: light:	ETS-4 UV	ETS-4 visible	ETS-10 UV[b]	ETS-10 visible	P25 UV[b]	P25 visible
P	0.04 (ISS)	0.00 (ISS)	0.08 (−ISS)	0.03 (−ISS)	2.77 (BG)	0.03 (−)
THB	1.30 (bg)	0.00 (−)	0.38 (bg + CT)	0.12 (CT)	5.74 (BG + CT)	0.22 (CT)
DHN	1.19 (bg)	0.00 (−)	4.46 (bg + CT)	0.30 (CT)	7.90 (BG + CT)	1.58 (CT)

[a] In parentheses is reported the degradation mechanism operating: BG = band gap; CT = charge transfer. When small letters are used (bg or ct), the mechanism is supposed to be present but with a low efficiency. When the inverse shape selectivity prevents the photodegradation, label ISS is added. [b] Values from ref 12.

irradiation with UV light, is the BG one. Conversely, both ETS-4 and ETS-10 exhibit a marked selectivity toward larger molecules, the photodegradation activities being in the order TCP > DCP > CP. When the photocatalytic experiments (Table 2) are combined with the UV−Vis spectra of the adsorbed complexes (Figure 11), the following can be noted. As the adsorption of TCP on both ETS-4 and ETS-10 causes only a small red shift of the absorption band, without resulting in a well-defined HOMO → LUMO transition band, the high efficiency of both photocatalysts to degrade TCP is explained by assuming that the $E_{LUMO} \approx E_c$ alignment is extremely good for both TCP/ETS-4 and TCP/ETS-10 systems. According to the data reported in Table 2, we conclude that this alignment is progressively less efficient for the DCP/ETS-4, DCP/ETS-10, and CP/ETS-10 systems and not operating at all for the CP/ETS-4 system, which shows all a well-defined HOMO → LUMO transition band (Figure 11). In all these cases a small contribution from the BG mechanism is certainly also present.

Note that these results have been explained for ETS-10 in terms of an inverse shape-selective behavior as the small molecules, able to penetrate inside the channels, are prevented from the degradation that occurs at the external surfaces where larger molecules are preferentially adsorbed.[11,12] The same model is able to explain the data for ETS-4, where the zeolitic protection acts on the small molecules able to be hosted inside the pockets or at the mouth of the channels. Adsorbates with shapes not fitting well in the available space at the mouths must be hosted on external surfaces where they are degraded faster.

6.2. Competitive Photodegradation of (Poly)hydroxylated Aromatic Compounds. Other interesting results are obtained studying the photodegradation of hydroxylated aromatic compounds such as P, THB and DHN on the three Ti-based photocatalysts. The experimental data are reported in Table 3.

Starting from P25 we observe that, conversely to the cases of (poly)chlorinated aromatic compounds (Table 2), selectivity is operative in a modest way when a cutoff filter at 310 nm is used but in a relevant way exciting in the visible region only (cutoff filter at 400 nm). As the P/P25 system is almost not degraded using visible light, unable to promote the BG mechanism, we conclude that the band alignment is similar to the case reported in complex B of Figure 10. Note also that surface phenates complexes have no appreciable absorption in the visible (see Figure 12). Consequently, when UV light is used, the degradation of P over P25 is explained in terms of the BG mechanism only. Coming to the THB/P25 and DHN/P25 systems irradiated with UV light, the higher activity of DHN is explained in terms of the additional role played by the "CT" mechanism; that is more efficient in the latter case. This interpretation is confirmed by the fact that, upon quenching the BG mechanism (visible excitation), both THB and DHN molecules are degraded on P25, according to the same trend.

Coming to the zeolitic titanosilicates, as already reported,[11,12] the photodegradation of small molecules such as P is prevented by the inverse shape-selectivity (Table 3). The case of ETS-4 is easily explained because the absence of any activity toward both THB and DHN molecules, when visible light is used, implies that the CT mechanism is not operative here (B-like band alignment in Figure 10), although a well-defined HOMO → LUMO band is present in both cases (Figure 12a). This hypothesis is further confirmed by the absence of selectivity observed when the BG mechanism is switched on by using the UV excitation source: $(r_{THB}/r_{DHN})_{ETS4} = 1.09$. Conversely, for both THB/ETS-10 and DHN/ETS-10 systems, the CT mechanism plays the dominant role, being slightly supported by the BG one. For the DHN/ETS-10 system we have considered that visible light is able to excite only the transition HOMO → LUMO due to the band at 21000 cm^{-1} (Figure 12b and Table 1) while with UV−Vis light it is possible to promote also the electronic transition of the band at higher frequencies (25000 cm^{-1}). This consideration explains the important drop in activity observed for the THB/ETS-10 system when moving from UV to Visible excitation light.

6.3. General Considerations Arising from the Whole Set of Photocatalytic Experiments. Further evidence on the relative reactivity of the studied materials, on the role of the CT and BG mechanisms, and on the relevance of the inverse shape selectivity claimed for microporous titanosilicates arises when considering all the investigated molecules together. In Figure 13 are plotted, normalized with regard to phenol rate (r_x/r_P), the data obtained on ETS-10 (squares) and P25 (circles) using the UV and the visible lights, parts (a) and (b), respectively. Data obtained on ETS-4 could not be included in the plot because $r_P = 0$ when the visible light is used.

In Figure 13a, the data have been ordered as a function of the increasing relative photodegradation efficiency when ETS-10 is used as photocatalyst: P, CP, DCP, THB, TCP, and DHN (Figure 13a). The relative photodegradation scale, obtained for ETS-10, basically corresponds to the relative molecule dimension. This means that, as already claimed before,[11,12] the inverse shape selectivity plays a fundamental

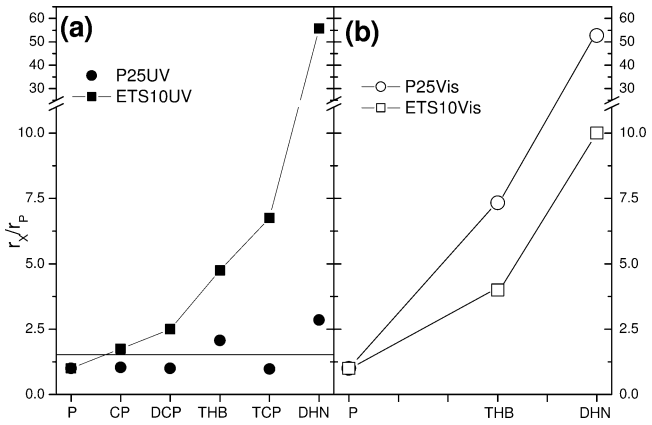

Figure 13. Disappearance rate ratio (r_x/r_P) of the different molecules obtained on ETS-10 (squares) and on P25 (circles): Parts (a) and (b) refer to photodegradation experiments performed with UV and visible photons, respectively. The molecules on the abscissa axis have been ordered according to the increasing r_x/r_P ratio observed on ETS-10 irradiated with UV photons. This order basically matchs with the increasing molecules size.

role in ETS-10. The important increase in the relative photodegradation efficiency obtained by moving from TCP ($r_x/r_P = 7$) to DHN ($r_x/r_P = 56$) cannot be explained in terms of inverse shape selectivity only, but needs the additional contribution of an efficient CT mechanism (see Table 2 and Table 3). In this regard, it is worth noticing that the adsorption of DHN on ETS-10 causes a significant modification of the electronic structure of both the solid and the molecule, resulting in the appearance of a strong absorption in the 30000−18000 cm^{-1} range (Figure 12b and Table 1). The spectrum reported in Figure 12b implies that the adsorbed DHN molecules are easily excited by UV−Vis photons. Moreover, the high value of r_{DHN}/r_P reported in Figure 13a implies also that an excellent band alignment is present for the DHN/ETS-10 system; see Figure 10 (complex A). These conclusions are supported by the data obtained on P25 (Figure 13a) that basically does not show any significant selective photodegradation. This is due to the fact that (i) no shape selectivity can be invoked here and (ii) the strong efficiency of the BG mechanism for P25 (exhibiting a much lower E_g) overshadows the effects of the CT mechanism.

The sub-band-gap excitation, where only the CT mechanism is operating (Figure 13b), is a mean to make P25 selective: $r_{THB}/r_P = 7$ and $r_{DHN}/r_P = 53$. Again, the absence of any possible shape selectivity on the titania surface implies that the differences observed for P, THB, and DHN on P25 irradiated with visible light is due to the selectivity associated with the CT mechanism. When absorbed on the titania surface, both THB and DHN molecules exhibit an important absorption in the visible range (Figure 12c). This means that both adsorbates are easily excited by visible radiation. The results of the photocatalytic experiments (Table 3 and Figure 13) indicate that a better band alignment occurs for the P25/DHN system, being that of the P25/THB still operative. The low efficiency in the degradation of P is easily explained in terms of the weak visible absorption of adsorbed P molecules, and to a nonefficient band alignment. The case of ETS-10 irradiated with visible light is more complex as the inverse shape selectivity and the CT selectivity act simultaneously. We will just comment that the trend observed with UV irradiation qualitatively still holds for the visible experiments.

7. Conclusions

In this work we combine a deep structural, vibrational, and electronic characterization of ETS-4 and ETS-10 photocatalysts with a complete study on the ability of the two titanosilicates to degrade a large set of organic pollutants using both UV and visible lights, able to excite above and below the materials energy gap, respectively. In all cases comparison with the standard titania (P25) is made. While microporous ETS-4 and ETS-10 exhibit a significant selectivity in the photodegradation of the above-mentioned molecules using both lights, P25 selectivity is observed with visible light only. We conclude that besides the inverse shape selectivity effect already observed for the microporous materials,[11,12] selectivity may be achieved also by selecting the excitation light in accordance with the electronic transition of the adsorbed molecule (determined by a previous systematic UV−Vis study). In such a case the photodegradation may occur if the conduction band of the Ti-based material is opportunely matched with the LUMO level of the adsorbed molecule so that it can receive the electron of the excited adsorbate. The concept of band alignment, well-established in the field of solid-state physics applied to semiconductor heterostructures,[78−80] is transferred to the field of photocatalysis for the first time.

Acknowledgment. We are indebted to Dr. G. J. Vitillo for the volumetric measurements reported in Figure S1 and for the graphical outputs reported in Figure 1, Figure 3, and Figure 4. Thanks are also due to Dr. F. Bonino for her kind support during Raman experiments (Figure 6) and to F. Cesano for the TEM study (Figure 2). The financial support of NATO programme for security through science "*Science for Peace Proposal* (SFP n. 981476) is gratefully acknowledged."

Supporting Information Available: Additional experimental section including text and figures. This material is available free of charge via the Internet at http://pubs.acs.org.

CM052841G